Available online at www.sciencedirect.com

ScienceDirect

International Journal of Heat and Mass Transfer 50 (2007) 2912–2923

International Journal of HEAT and MASS TRANSFER

www.elsevier.com/locate/ijhmt

A numerical investigation on the influence of liquid properties and interfacial heat transfer during microdroplet deposition onto a glass substrate

Rajneesh Bhardwaj [a], Jon P. Longtin [b], Daniel Attinger [a,*]

[a] Laboratory for Microscale Transport Phenomena, Department of Mechanical Engineering, Columbia University, New York, NY 10027, United States
[b] Thermal-Laser Laboratory, Department of Mechanical Engineering, State University of New York at Stony Brook, Stony Brook, NY 11794, United States

Received 2 November 2006; received in revised form 18 December 2006
Available online 2 March 2007

Abstract

This work investigates the impingement of a liquid microdroplet onto a glass substrate at different temperatures. A finite-element model is applied to simulate the transient fluid dynamics and heat transfer during the process. Results for impingement under both isothermal and non-isothermal conditions are presented for four liquids: isopropanol, water, dielectric fluid (FC-72) and eutectic tin–lead solder (63Sn–37Pb). The objective of the work is to select liquids for a combined numerical and experimental study involving a high resolution, laser-based interfacial temperature measurement to measure interfacial heat transfer during microdroplet deposition. Applications include spray cooling, micro-manufacturing and coating processes, and electronics packaging. The initial droplet diameter and impact velocity are 80 μm and 5 m/s, respectively. For isothermal impact, our simulations with water and isopropanol show very good agreement with experiments. The magnitude and rates of spreading for all four liquids are shown and compared. For non-isothermal impacts, the transient drop and substrate temperatures are expressed in a non-dimensional way. The influence of imperfect thermal contact at the interface between the drop and the substrate is assessed for a realistic range of interfacial Biot numbers. We discuss the coupled influence of interfacial Biot numbers and hydrodynamics on the initiation of phase change.

Keywords: Microfluidics; Drop impact; Interfacial heat transfer; Numerical simulation; Thermoreflectance technique

1. Introduction

The fluid dynamics and heat transfer associated with microdroplet impingement onto a solid substrate are of considerable interest to micro-manufacturing, spray cooling, spray coating, and inkjet-printing [1–3]. A variety of fluids are used in such processes, including fuels in combustion, water and dielectric fluids for cooling, and metal droplets for rapid prototyping and electronic interconnects [4,5].

In this work a numerical investigation of a liquid microdroplet impacting on a horizontal substrate at different temperatures is presented (Fig. 1). The initial droplet diameter and impact velocity are 80 μm and 5 m/s, respectively and gravity is negligible. The associated transport phenomena are extremely complex. For instance, this problem involves fluid dynamics with large deformations of the droplet free surface. The simultaneous, transient heat transfer process involves convection in the droplet coupled with conduction in the substrate. Both the thermal field inside the droplet and the onset of phase change, if any, depend on the interfacial heat transfer coefficient between the droplet and substrate, which expresses the imperfect thermal contact at the interface. Our study focuses on drops of eutectic tin–lead solder (63Sn–37Pb, referred as solder, hereafter), water, isopropanol and FC-72 fluorocarbon, a dielectric fluid used for electronics cooling. A primary objective of this work is to evaluate these liquids as

---

* Corresponding author. Tel.: +1 212 854 2841; fax: +1 212 854 3304.
E-mail address: da2203@columbia.edu (D. Attinger).

0017-9310/$ - see front matter © 2007 Elsevier Ltd. All rights reserved.
doi:10.1016/j.ijheatmasstransfer.2006.12.015

Nomenclature

Bi	Biot number ($h_c d_0 k_l^{-1}$)
c	speed of sound (m s^{-1})
c_p	specific heat (J kg^{-1} K^{-1})
C	dimensionless heat capacity ($\rho c_p/\rho_l c_{p,l}$)
d	splat diameter (m)
e	distance of center of circular measurement spot from origin on r-axis (m)
Fr	Froude number ($v_0^2 d_0^{-1} g^{-1}$)
g	gravitational acceleration (9.81 m s^{-2})
h	interfacial heat transfer coefficient (W m^{-2} K^{-1})
H	mean surface curvature (m^{-1})
$\overline{H}$	dimensionless mean surface curvature (Hd_0)
k	thermal conductivity (W m^{-1} K^{-1})
K	dimensionless thermal conductivity (kk_l^{-1})
M	Mach number ($v_0 c^{-1}$)
n	number of grid points inside circular measurement spot
p	pressure (Pa)
P	dimensionless pressure ($pv_0^{-2}\rho_l^{-1}$)
Pr	Prandtl number ($\mu c_{p,l} k_l^{-1}$)
q	heat flux at the splat/substrate interface (W m^{-2})
r	radial coordinate (m)
R	dimensionless radial coordinate (rd_0^{-1})
Re	Reynolds number ($\rho v_0 d_0 \mu^{-1}$)
s	radius of spot (m)
t	time (s)
T	temperature (K)
u	radial velocity (m s^{-1})
U	dimensionless radial velocity (uv_0^{-1})
v	axial velocity (m s^{-1})
V	dimensionless axial velocity (vv_0^{-1})
We	Weber number ($\rho v_0^2 d_0 \gamma^{-1}$)
z	axial coordinate (m)
Z	dimensionless axial coordinate (zd_0^{-1})

Greek symbols

α	thermal diffusivity (m^2 s^{-1})
β	spread factor ($d_{\max}\, d_0^{-1}$)
δt	temporal resolution available by experimental setup
γ	surface energy (J m^{-2})
ϕ	contact angle
μ	dynamic viscosity (Pa s)
θ	dimensionless temperature ($\{T - \min(T_{1,0}, T_{2,0})\}(\lvert T_{1,0} - T_{2,0}\rvert)^{-1}$)
ρ	density (kg m^{-3})
σ	stress (Pa)
τ	dimensionless time ($tv_0 d_0^{-1}$)

Subscripts

0	initial
1	drop/splat
2	substrate
avg	average value
c	contact, interface
i	initial
int	linearly interpolated value
l	liquid
max	maximum value
r	radial direction
z	axial direction

potential candidates for a companion experimental study, currently being developed, to measure interfacial heat transfer coefficients and temperature history and compare the results to numerical simulations.

Traditionally, numerical models targeting similar problems use strong simplifications for the sake of numerical tractability [3]. For instance Harlow and Shannon [6] neglected both viscous and surface tension effects in their modeling of a liquid droplet impacting on a flat plate. Tsurutani et al. [7] used the simplified marker and cell method (SMAC) and employed a fixed grid with relatively low resolution. Increasing computing capacities have recently led to very convincing simulations of the impact of millimeter-size drops with the Volume-Of-Fluid method [8], however the ability of this technique to address micrometer-size droplet cases, where free surface effects are more important, is not assessed yet. Gao and Sonin [9] developed a powerful theoretical analysis in which order-of-magnitude approximations were made to characterize the associated time scales, such as the times required to remove the initial superheat, remove the latent heat during freezing, and subsequently cool the deposit to the ambient temperature. Two effects that have been shown to be significant in other studies were neglected in this formulation: *convection effects* within the droplet and *thermal contact resistance* at the splat-substrate interface [10,11].

Zhao et al. [12] modeled the cooling of a liquid microdroplet, accounting for fluid dynamics phenomena and assuming perfect interfacial thermal contact. This group used a Lagrangian formulation, extending the fluid dynamics model of Fukai et al. [13] to account for the heat transfer process in the droplet and substrate. Wadvogel et al. [14,15] extended this modeling to account for solidification and imperfect interfacial thermal contact. This modeling is used in this article, with the incorporation of a more stable and versatile mesh generation scheme *Mesh2d* [16], and the ability to modify the interfacial heat transfer coefficient with respect to time and space.

Several studies have specifically investigated the role and importance of imperfect thermal contact between the substrate and the drop. This imperfect thermal contact is a critical parameter in the heat transfer process. Liu et al.

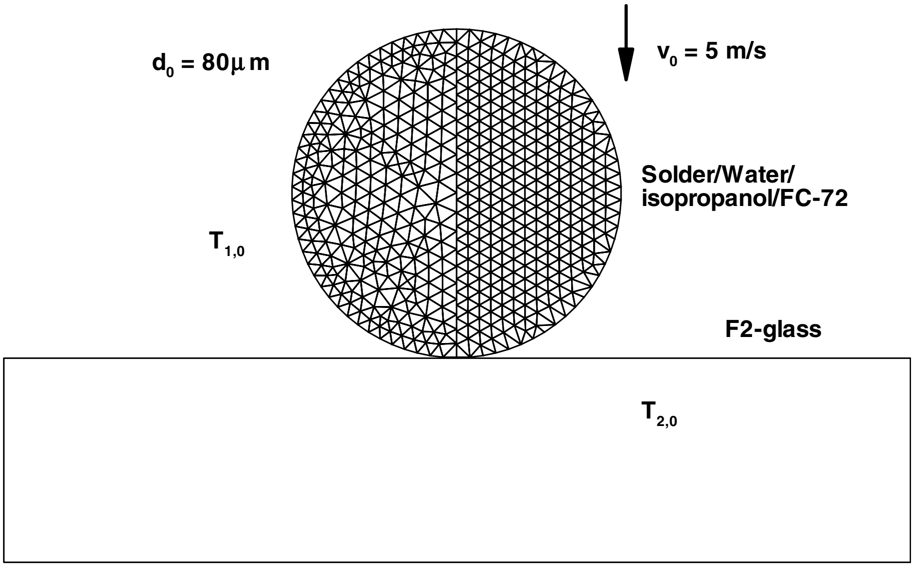

Fig. 1. Problem definition.

[17] suggest that when a liquid spreads over a solid surface, perfect thermal contact cannot be achieved between the liquid and solid surface because of the substrate surface roughness, surface tension, surface impurities, and gas entrapment. It is believed that heat transfer through the actual (imperfect) contact area occurs by conduction and, to some degree, radiation across the gas-filled gaps [3]. For molten lead droplets, imperfect thermal contact was experimentally observed by Bennett and Poulikakos [11]. Pasandideh-Fard et al. [18] and Xiong et al. [19] performed a numerical study on the sensitivity to contact resistance on the final diameter, overall shape and height of a solidified solder droplet. Their model predicted variations in solders bump height up to 20% due to variations of thermal contact resistance. Recently, Attinger and Poulikakos [20] compared experimental and numerical transient oscillations for a solidifying solder drop and were able to estimate the value of the interfacial heat transfer coefficient for a specific case. Although the investigations above have shown the importance and effects of the interfacial heat transfer coefficient, there is still a lack of modeling and predictive tools to determine *a priori* the interfacial heat transfer coefficient.

This study is aimed at selecting liquids and temperatures for a combined theoretical and experimental investigation of fluid dynamics and heat transfer during the impact of microdroplet on a solid surface at different temperature. The laser-based technique developed by Chen et al. [21] will be modified and used to measure the interfacial temperature with microsecond and micrometer resolution under a spreading droplet. Matching the measured and calculated temperature values at the interface will allow the determination of the transient and local behavior of the heat transfer coefficient, which is a necessary step in developing predictive models for interfacial heat transfer. In this article, we discuss the effect of interfacial heat transfer on the heat transfer process during the impact of solder, water, isopropanol and FC-72 (dielectric fluid) droplets on a glass substrate.

2. Numerical model

The mathematical model is based on the Navier–Stokes and energy equations [14] applied to an axisymmetric geometry. All equations are expressed in a Lagrangian framework, which provides accurate modeling of the large deformations of the free surface and the associated Laplace stresses [13].

2.1. Fluid dynamics

The flow inside the droplet is laminar and all thermophysical properties are assumed to be constant with respect to temperature. The radial and axial components of the momentum equation are considered along with the continuity equation. An artificial compressibility method is employed to transform the continuity equation into a pressure evolution equation. This method assumes a fluid flow that is slightly compressible, whereby the speed of sound is large, but not infinite. A Mach number of 0.001 is used for all simulations in this work. The derivation of the boundary condition at the free surface considers forces due to pressure, viscous stresses and surface tension [13]. The traditional no-slip boundary condition fails in the vicinity of the contact line because its application results in an infinite stress in the region. To circumvent this problem, a scheme proposed by Bach and Hassager [22] is utilized, which applies a net interfacial force given by the equilibrium surface tension coefficient of the joining phases. The wetting force at the dynamic contact line between the liquid droplet and the substrate is neglected throughout the analysis. The dimensional form of the fluid dynamics equations can be found in [23], with the expression of the stress tensor. The dimensionless equations for fluid dynamics are [15]:

2.1.1. Mass conservation

$$\frac{\partial P}{\partial \tau}+\frac{1}{M^2}\left(\frac{1}{R}\frac{\partial}{\partial R}\left(RU+\frac{\partial V}{\partial Z}\right)\right)=0 \tag{1}$$

where P, τ, R, Z, U, V are dimensionless pressure, time, radial distance, axial distance, radial velocity and axial velocity, respectively. M denotes Mach number.

2.1.2. Momentum conservation in radial direction

$$\frac{\partial U}{\partial \tau}-\frac{1}{R}\frac{\partial}{\partial R}(R\bar{\sigma}_{RR})-\frac{\partial \bar{\sigma}_{RZ}}{\partial Z}+\frac{1}{R}\bar{\sigma}_{\theta\theta}=0 \tag{2}$$

where $\bar{\sigma}_{RR}$ and $\bar{\sigma}_{ZZ}$ are dimensionless stress tensor terms which include both viscous and free surface stresses [15].

2.1.3. Momentum conservation in axial direction

$$\frac{\partial V}{\partial \tau}-\frac{1}{R}\frac{\partial}{\partial R}(R\bar{\sigma}_{ZR})-\frac{\partial \bar{\sigma}_{ZZ}}{\partial Z}+\frac{1}{Fr}=0 \tag{3}$$

In the above equation, Fr denotes Froude number.

2.2. Heat transfer

The energy equation is solved in both the droplet and the substrate, according to the formulation in [15]. Convection and radiation heat transfer from all exposed surfaces is neglected. The dimensionless energy conservation equation for droplet and substrate is given by ($i = 1$ for droplet and $i = 2$ for substrate):

$$C_i\frac{\partial \theta_i}{\partial \tau}-\frac{1}{PrRe}\left[\frac{1}{R}\frac{\partial}{\partial R}\left(K_iR\frac{\partial \theta_i}{\partial R}\right)+\frac{\partial}{\partial Z}\left(K_i\frac{\partial \theta_i}{\partial Z}\right)\right]=0 \tag{4}$$

where C_i and K_i is the dimensionless heat capacity and thermal conductivity, respectively. Pr and Re denotes Prandtl and Reynolds number, respectively. θ_i is the dimensionless temperature, and is defined as:

$$\theta_i=\frac{T_i-\min(T_{1,0},T_{2,0})}{|T_{1,0}-T_{2,0}|} \tag{5}$$

where $T_{1,0}$ and $T_{2,0}$ are the initial dimensional temperature of drop and substrate, respectively.

2.3. Thermal contact resistance

Thermal contact resistance between droplet and substrate is modeled by a thin layer of arbitrary thickness δ, with zero heat capacity and adjustable thermal conductivity k_i [19]. The interfacial heat transfer coefficient can therefore be defined as $h_\mathrm{c}=k_\mathrm{i}/\delta$. This approach is fully compatible with that of Wang and Matthys [24]. The interfacial heat transfer coefficient can be non-dimensionalized as the interfacial Biot number [19]:

$$Bi=\frac{h_\mathrm{c}d_0}{k_1} \tag{6}$$

where d_0 is the initial diameter of the droplet.

2.4. Initial and boundary conditions

The initial conditions are as follows:

$$U=0;\quad V=-1;\quad P=\frac{4}{We} \tag{7}$$

$$\theta_1(R,Z,0)=1;\quad \theta_2(R,Z,0)=0\quad \text{for solder} \tag{8}$$

$$\theta_1(R,Z,0)=0;\quad \theta_2(R,Z,0)=1\quad \text{for water, isopropanol and FC-72} \tag{9}$$

The last two initial conditions show that the solder drop is cooled upon contact with the substrate, while water, isopropanol and FC-72 drops are heated.

The boundary conditions are as follows:

$$U=0;\quad \frac{\partial V}{\partial R}=0\quad \text{at } R=0 \tag{10}$$

$$U=V=0\quad \text{at}\quad Z=0 \tag{11}$$

$$\overline{\sigma_{RR}}n_R+\overline{\sigma_{RZ}}n_Z=-2\frac{\overline{H}}{We}n_R\quad \text{at droplet free surface} \tag{12}$$

$$\overline{\sigma_{ZR}}n_R+\overline{\sigma_{ZZ}}n_Z=-2\frac{\overline{H}}{We}n_Z\quad \text{at droplet free surface} \tag{13}$$

The above two boundary conditions are the balance of forces due to pressure, viscous stresses and surface tension at droplet free surface.

$$\frac{\partial \theta_i}{\partial R}n_r+\frac{\partial \theta_i}{\partial Z}n_z=0\quad \text{at droplet free surface and the substrate boundary surface} \tag{14}$$

3. Numerical scheme

The computational domain is discretized as a mesh of triangular elements and the numerical model is solved using a Galerkin finite element method. Linear shape functions are used for velocity and pressure. An implicit method is utilized for the integration of fluid dynamics equations in time, while a Crank–Nicholson scheme is used for the energy equation. Details of the algorithm are given in [15]. The present model uses a more robust and freely available mesh generator *Mesh2D* [16]. It has been found that *Mesh2D* is better than the advancing front method [25] in terms of the time taken to generate mesh, the allowable aspect ratio of the elements, and the number of elements generated. A comparison of meshes generated by two methods is shown in Fig. 1.

In the present work, the grid and time step independence are examined in terms of the height of splat along z-axis, Z_c as shown in Fig. 2. This study is carried out for 80 μm solder droplet impacting a flat surface at 5.0 m/s under isothermal conditions. This corresponds to $Re = 1254.7$ and

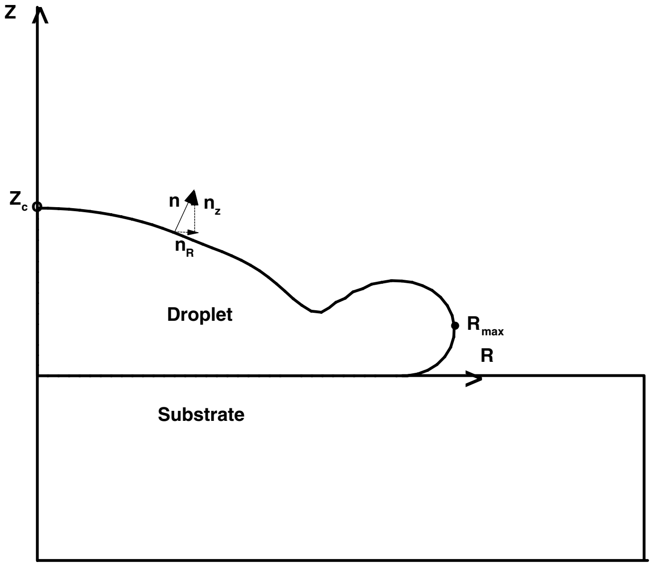

Fig. 2. Axisymmetric droplet coordinate definition.

$We = 32.4$. The grid independence is considered for four increasing number of nodes in the droplet: 199, 521, 705 and 873, with a time step of 5×10^{-4} in each case. The time step independence is considered for time steps of 0.5, 1, 2, and 3×10^{-3} for 705 nodes in each case, with the results shown in Fig. 3. As it can be seen, a time step of 5×10^{-4} and a spatial discretization of 700 nodes in the droplet are sufficient to guarantee the grid and time step independency of the simulations. Each simulation requires approximately 6 CPU hours on a 2.4 GHz Intel-Xeon machine with 1 GB of RAM.

3.1. Thermophysical properties and dimensionless numbers

The thermophysical properties and dimensionless numbers used for simulations are given in Tables 1 and 2, respectively. While the numerical code can accommodate temperature-dependent thermophysical properties, this dependence is not considered in this study where the behavior of four fluids is expressed in terms of dimensionless temperature for the sake of generality and ease of comparison between fluids. The validity of assuming constant properties can however be evaluated by determining the temperature interval ΔT where the variation of two main physical properties, the surface tension and viscosity, is within 10%, using data in [26,27]. Surface tension stays constant within 10% for a ΔT of 45, 30, 25, 29 and 11 °C in the respective cases: water cooled to ambient temperature, water heated to boiling temperature, isopropanol cooled to ambient temperature, isopropanol heated to boiling point and FC-72 heated to its evaporation point. For the same respective cases, viscosity stays constant within 10% for respective ΔT of 7, 8, 5, 13 and 11 °C. For solder cooled to its melting point, viscosity stays constant within 10% for ΔT of 65 °C, while surface tension only experiences a change of 2% over the same interval.

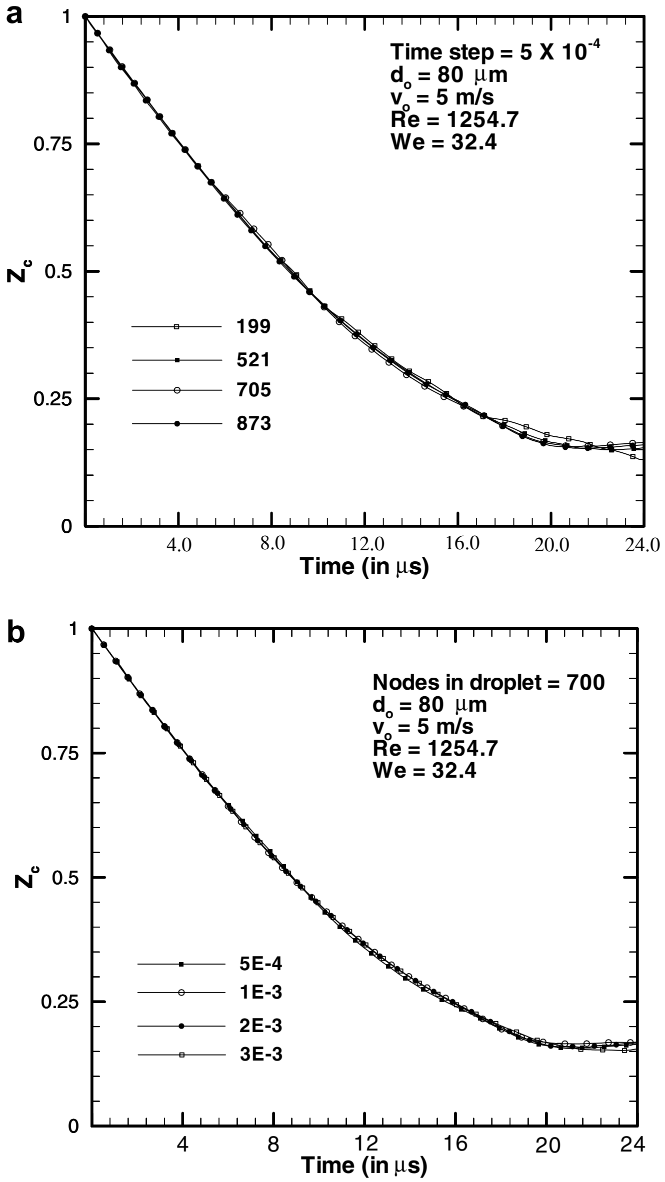

Fig. 3. (a) Grid independence study: variation of height of splat in z-axis with time for different numbers of nodes in the splat; (b) time-step independence study: variation of height of splat in z-axis with time for different time steps.

4. Results and discussion

Results are presented for solder, water, isopropanol and FC-72 droplets with diameter $d_0 = 80\ \mu m$; velocity $v_0 = 5\ m/s$ and values of Bi of 1, 10 or 100. This choice of Biot numbers represents a realistic range of values used in previous work [19]. The initial temperatures are dimensionless, which means that a single simulation result describes any non-isothermal impact. In case of solder the droplet is cooled by the substrate, so the initial dimensionless temperatures for drop and substrate are 1

Table 1
Thermophysical propeties used in the simulations

Droplet	Density (kg m^{-3})	Thermal conductivity (W m^{-1} K^{-1})	Specific heat (J kg^{-1} K^{1})	Viscosity (Pa s)	Surface energy (J m^{-2})	Initial dimensionless temperature	Thermal diffusivity (m^2 s^{-1})
Solder	8218	25	238	2.6×10^{-3}	0.507	1.0	1.28×10^{-5}
Water	997	0.607	4180	9.8×10^{-4}	7.3×10^{-2}	0.0	1.46×10^{-7}
Isopropanol	785	0.17	3094	2.5×10^{-3}	2.1×10^{-2}	0.0	7.0×10^{-8}
FC 72	1680	0.055	1050	6.4×10^{-4}	1.0×10^{-2}	0.0	3.1×10^{-8}
Substrate							
F2 glass	3618	0.78	557	–	–	0.0 (solder); 1.0 (water, isopropanol and FC-72)	3.87×10^{-7}

Table 2
Dimensionless numbers for drops of different liquids

Droplet	*Re*	*We*	*Pr*	*Bi*
Solder	1254.7	32.4	2.5×10^{-2}	1, 10 or 100
Water	407.4	27.4	6.7	1, 10 or 100
Isopropanol	128.2	73.9	44.6	1, 10 or 100
FC-72	1050.0	336.0	12.2	1, 10 or 100

and 0, respectively. In the cases where water, isopropanol and FC-72 droplets are heated by the substrate, these corresponding values are 0 and 1.

4.1. Fluid dynamics

Fig. 4 shows the spreading of a solder microdroplet with successive representations of the droplet shape, temperature isotherms, and streamlines. During the initial spreading stage ($t < 12\ \mu s$), the deformation of the drop is mostly influenced by inertial forces. However, in the later stages of spreading ($t > 25\ \mu s$), inertial forces decrease and surface tension forces dominate. This competition between inertial and surface tension forces induces the peripheral ring visible for $t = 20\ \mu s$, as well as a strong recoiling which results in the splashing of the solder drop. Also a vortex forms in the drop during recoiling (Fig. 4).

4.1.1. Comparison of spreading in all four liquids

The temporal evolution of the spread factor β (ratio of maximum splat diameter to initial droplet diameter) for all four liquids is plotted in Fig. 5. The least spreading is observed with solder, which is due to its small Weber number (Table 2). The maximum spreading occurs with FC-72 because of its large Weber number. In general, a larger Weber number results in more substantial droplet spreading.

4.1.2. Comparison with previous results

Recently our numerical code was validated with experimental results for solder [20]. In the present work, numerical values of the maximum spread factor for water and isopropanol are compared with visualization results [28], and also with analytical expressions available in the literature [18]. In Table 3, we use the same parameters as in the visualization study [28]: for isopropanol the parameters are $d_0 = 87\ \mu m$ and $v_0 = 9.28\ m/s\ (Re = 259, We = 277)$. For water, the parameters are: $d_0 = 83\ \mu m$ and $v_0 = 8.19\ m/s\ (Re = 696, We = 77)$. The analytical estimate for the maximum value of the spread factor (β_{max}) in [18] assumes that the surface energy at the maximum spreading equals the kinetic and surface energy before impact, less the viscous dissipation during impact:

$$\beta_{max} = \frac{d_{max}}{d_0} = \sqrt{\frac{We + 12}{3(1 - \cos\phi) + 4\frac{We}{\sqrt{Re}}}} \qquad (15)$$

where ϕ is contact angle.

Table 3 shows very good agreement between numerical, experimental and analytical results. The lower value obtained analytically for the maximum spread factor of isopropanol may be explained by the fact that the lower Reynolds number related to the isopropanol impact does not fully match the assumption in Eq. (15) that viscous dissipation is due to an established boundary layer between the drop and the substrate. The viscous dissipation term in Eq. (15) would thus require a modification for Reynolds numbers lower than 500 to incorporate this effect.

The maximum spread factor of isopropanol is greater than that for water due to its larger Weber number. For impact of a liquid with $We > 1$, the spreading process is driven by the radial pressure gradient induced by the sudden velocity change at the impact location [23]. After the maximum spread factor is reached, the water splat recoils (Fig. 5). The isopropanol case shows that less recoiling occurs after the maximum spread factor is attained.

4.2. Heat transfer

4.2.1. Effect of Biot number and drop properties

Fig. 6 shows the influence of the Biot number on the four liquids. As the Biot number increases, heat transfer occurs more rapidly between the substrate and the drop for all cases. This can be verified by the location of typical isotherms for $Bi = 1$ and 100. It is interesting to notice that

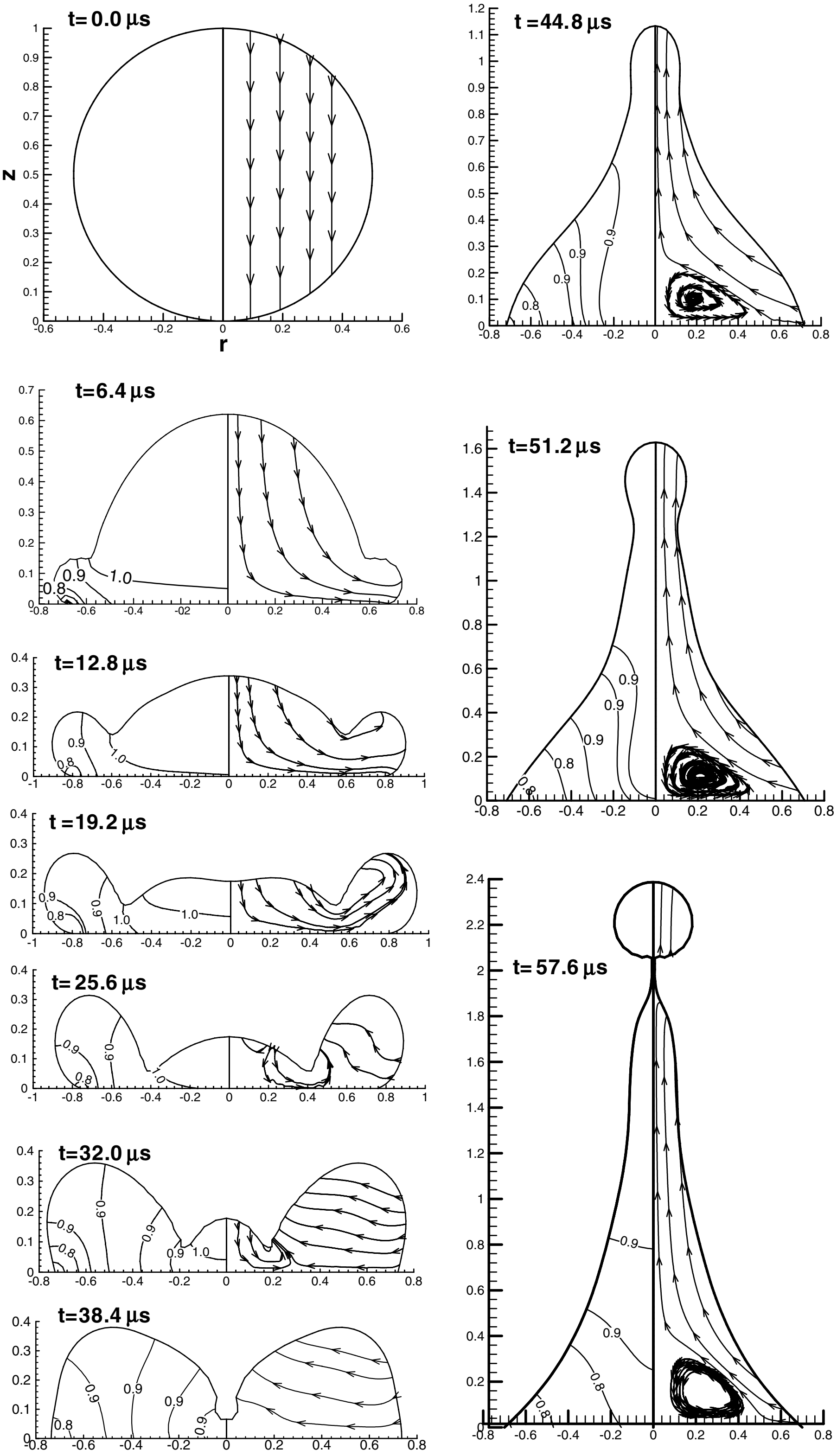

Fig. 4. Spreading, recoiling and splashing of a solder drop. Isotherms (on left hand side) and streamlines (on right hand side) are shown for 0.0–57.6 μs ($Bi = 100$). Splashing occurs at this latter time.

the temperature gradients in the solder drop are in the radial direction (Fig. 4), while water, isopropanol and FC-72 splats exhibit axial temperature gradients (Fig. 6). This is due to the higher thermal diffusivity of the solder (Table 1): during the impact, the solder drop assumes a doughnut shape, with high-temperature fluid continuously

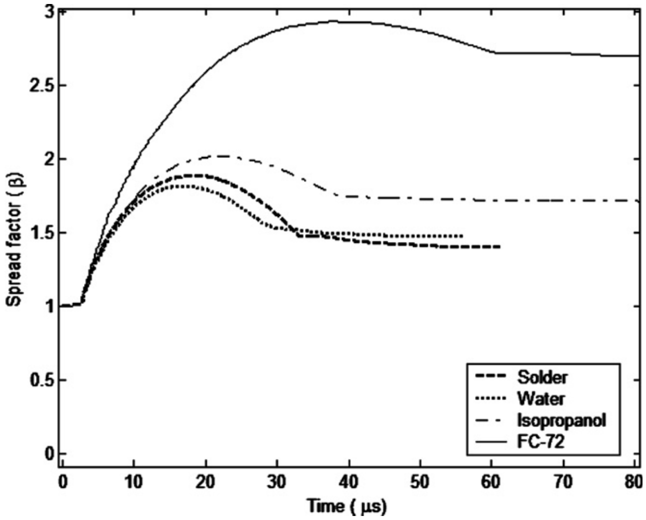

Fig. 5. Evolution of spread factors with time for all four liquids.

Table 3
Comparison of maximum spread factor with published results

Droplet	Maximum spread factor ($\beta_{\max}$)		
	Present work, numerical	Ref. [28], experimental	Ref. [18], analytical[a]
Water	2.41	2.45	2.44
Isopropanol	2.52	2.51	2.01

[a] Contact angle ϕ assumed to be 90° for water and isopropanol.

supplied to the center region, so that the splat periphery is rapidly cooled by contact with the low-temperature substrate. The association of this flow pattern and the higher thermal diffusivity results in radial temperature gradients (Fig. 4).

In later stages of spreading for isopropanol and FC-72, the heat flux across the interface is mainly governed by conduction through the substrate. The low values of thermal diffusivity (Table 1) for these two liquids result in axial thermal gradients for both.

The occurrence of phase change (if any) can be predicted from Figs. 4 and 6, e.g. in the case of solidification or initiation of Leidenfrost boiling. When the Biot number is large ($Bi = 100$), the largest temperature change is seen at the periphery of the solder drop while for the other three liquids the isotherms are horizontal. This implies that the solder drop will begin to solidify at its periphery first while the other three liquids will start to evaporate over the entire contact surface between the droplet and substrate. When $Bi \sim 1$, isotherms in Fig. 6 show that no significant heat transfer takes place between drop and substrate during the spreading phase.

4.2.2. *Effect of droplet liquid on temperature change in splat*

The thermal diffusivities of four liquids are listed in decreasing order in Table 1. Accordingly, variations of temperature inside the splat occur more rapidly for higher values of thermal diffusivities. This can be quantified analytically by considering the splat and substrate as semi-infinite bodies. The analytical solution of the transient 1D heat conduction problem in a semi-infinite medium that is initially at a uniform temperature $T_{1,0}$ and is put in contact

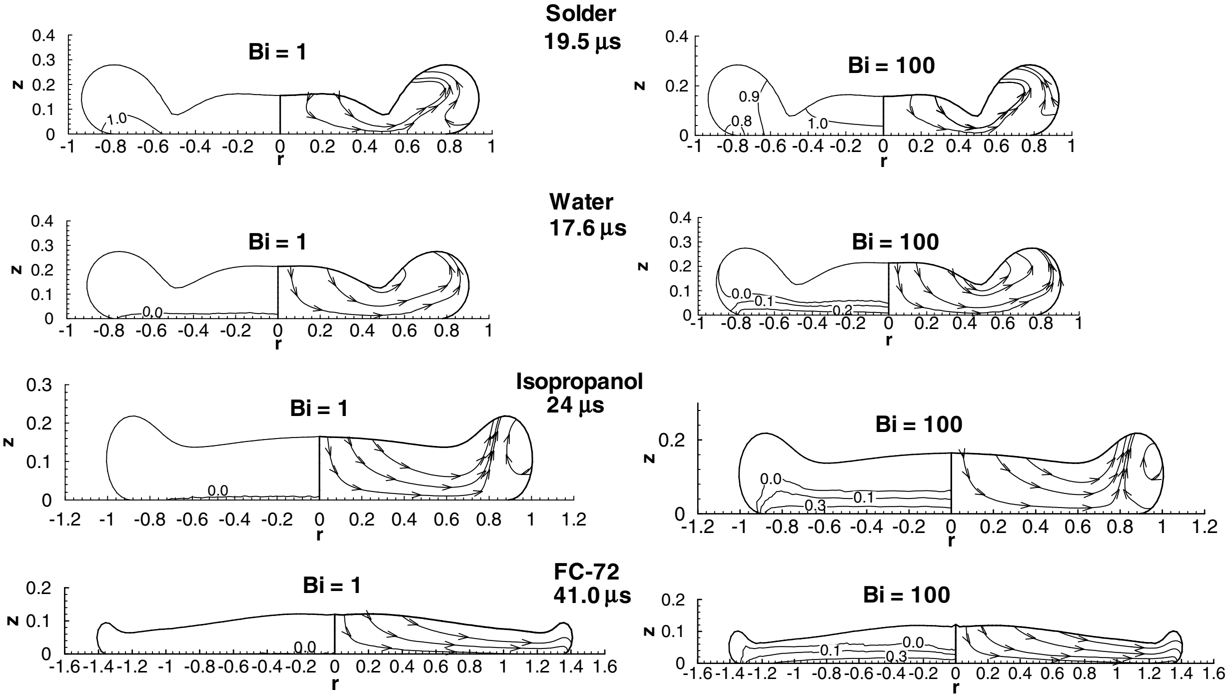

Fig. 6. Effect of Biot number on splat shape and temperature distribution for solder, water, isopropanol and FC-72. Isotherms (on left hand side) and streamlines (on right hand side) are shown at the maximum extension of spreading of corresponding splats.

Table 4
Comparison of axial thickness for a 20% temperature change in splat obtained by numerical and analytical approach

Droplet	Axial thickness (in μm), numerical	Axial thickness (in μm), analytical	Percentage error (%)
Water	1.04	0.96	10.58
Isopropanol	0.80	0.66	17.50
FC-72	0.72	0.47	34.72

at time $t = 0$ with a semi-infinite body at another temperature $T_{2,0}$ is [29]:

$$\frac{T(z,t) - T_{1,0}}{T_{2,0} - T_{1,0}} = \mathrm{erfc}\left(\frac{z}{2\sqrt{\alpha t}}\right) \tag{16}$$

Considering the splat as a semi-infinite medium and using the analytical approach in Eq. (16), we can determine analytically the axial splat thickness corresponding to a 20% temperature change at the time corresponding to the maximum extension of spreading (Table 4). For $Bi = 100$ this thickness is 0.96, 0.66 and 0.47 μm, for water, isopropanol and FC-72, respectively. Numerically, the thickness corresponding to a 20% change in temperature at the maximum extension of spreading can be determined from the simulations. These thickness values are 1.04, 0.80 and 0.72 μm for water, isopropanol and FC-72, respectively. In both the analytical and numerical approach, the time to reach the maximum spreading is obtained from the simulations as 18, 24 and 42 μs, for water, isopropanol and FC-72, respectively. Results for solder are not compared because thermal gradients are in the radial direction. The comparison between the analytical and numerical results for the thickness corresponding to a 20% change in temperature gives therefore reasonably consistent results (within 40% error, Table 4), provided the thermal diffusivity is not too large. In the case of solder for example, thermal diffusivity is about 1000 times higher than isopropanol and FC-72, which induces vertical isotherms: therefore no comparison is possible between the analytical model and the measurement in this case, but only comparison between the numerical calculation and the measurement.

5. Feasibility of experiments

A key objective of this work is to study the feasibility of using a recent laser-based temperature measurement technique [21] together with the numerical simulations. This coupled study will provide data with unprecedented temporal and spatial resolution on the behavior of interfacial heat transfer during droplet impingement on a substrate. The measurement technique is a laser-based thermoreflectance technique that measures the temperature at the fluid–substrate interface [21]. This technique is being modified to probe the temperature with an improved temporal resolution of 1 μs and a spatial resolution of 15 μm.

The setup is shown in Fig. 7. A low-power He–Ne laser and a silicon photodiode are used to monitor the real-time reflectivity of the interface Both the droplet and substrate have a temperature-dependent refractive index, with the result that temperature changes in the droplet and substrate induce a reflectivity change of a laser beam incident on the droplet–substrate surface. By measuring the change in intensity of light reflected from the interface, the temperature at the interface can be obtained. The measured temperature change ΔT is proportional to the photodiode voltage change ΔV and can be determined as follows [21]:

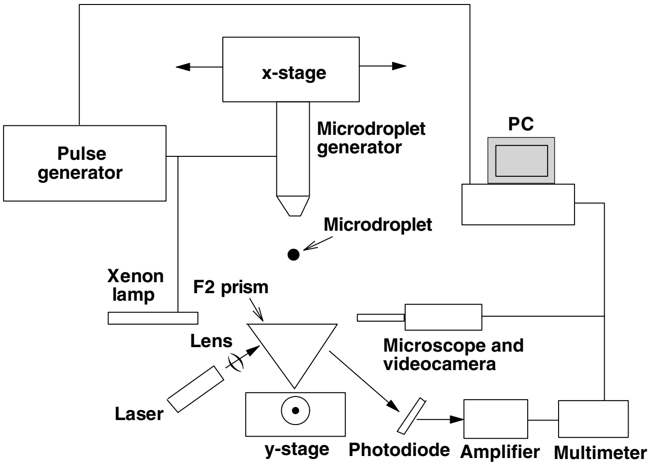

Fig. 7. A schematic diagram of proposed experimental set up.

$$\Delta T = \frac{R_0}{V_0\left[\frac{\partial R}{\partial n_l}\frac{\partial n_l}{\partial T} + \frac{\partial R}{\partial n_s}\frac{\partial n_s}{\partial T}\right]}\Delta V \tag{17}$$

where R is the reflectivity, n the refractive index, and subscripts l and s are liquid and substrate, respectively. Since $\frac{\partial n_s}{\partial T}$ is typically much less than $\frac{\partial n_l}{\partial T}$, the variation of substrate reflectance is negligible in comparison with the variation of droplet reflectance.

Such a non-intrusive method is an ideal candidate for local and transient interface temperature measurements. Matching experimental and numerical temperatures (with the Biot number as a parameter) will allow the determination of the interfacial heat transfer coefficient.

5.1. Selection of liquids

The determination of the most appropriate liquids for the determination of interfacial heat transfer coefficient can be helped by simulations showing how the temperature of the droplet–substrate interface evolves during impingement. Such information is shown in Figs. 4 and 6. For example, the solder splat exhibits strong variation of the interface temperature in the radial direction for Biot numbers in the range 100. Solder is thus a strong candidate for experiments focused on the spatial variation of interfacial heat transfer coefficient. On the other hand, both isopropanol and FC-72 spread more (18–37%) than solder (Fig. 6), which implies that a proportionally larger droplet area will be available for the laser measurement. It is worth mentioning that the spreading evolution (diameter at the interface vs. time) can be measured using the same laser technique. For water, the maximum spreading of 64 μm is relatively small and the radial interface temperature is moderate, which represents a combination of both the solder and isopropanol/FC-72 behavior. As a conclusion, isopropanol can be used for testing the method, while solder and FC-72 will be tested because of their practical relevance.

5.2. Error induced by the spatial and temporal resolution of the measurement

This numerical study also provides estimates of the needed spatial and temporal resolution of the laser measurement to accurately capture key features of the fluid and thermal dynamics. For example, the entire spreading and cooling of a solder drop takes less than 100 μs with maximum spreading diameter of 76 μm (Fig. 4). The experimental method is expected to provide an estimated temporal resolution of 1 μs and spatial resolution of 15 μm, corresponding to the circular laser spot at the droplet–substrate interface. It is worth estimating the error induced by the spatial-averaging due to the extension of the spot size, as well as the error induced by the time-averaging. This is shown in Fig. 9, where spatially averaged temperature profiles (as the measurement will provide) are compared with the temperatures obtained numerically at the expected center of the laser beam measurement. In the spatially averaged profile, numerical temperatures are averaged within successive 15 μm spot as follows (Fig. 8):

$$T_{\text{avg,spatial}} = \frac{\sum_{k=1}^{n}\{T_{k,\text{int}}(A_{k+1}-A_k)\} + A_1 T_{s1} + (\pi s^2 - A_n)T_{s2}}{\sum_{k=1}^{n}(A_{k+1}-A_k) + A_1 + (\pi s^2 - A_n)} \tag{18}$$

where n is number of grid points inside the spot; $T_{k,\text{int}}$ is the linearly interpolated temperature value at the middle of the segment joining two consecutive grid points: $T_{k,\text{int}} = (T_k + T_{k+1})/2$; T_{s1} and T_{s2} are the temperatures at the intersection of the r-axis and the circular measurement spot (Fig. 8). The area A_k is determined by the intersection of the circular spot and the disk defined by the k_{th} isotherm in the r–θ plane, located at a radial distance of r_k, and s is the radius of measurement spot. If e is distance between the spot center and the origin, A_k can be expressed as follows [30]:

Case I: If $r_k > |e - s|$, then

$$A_k = r_k^2\left(\cos^{-1}\frac{e^2 + r_k^2 - s^2}{2er_k}\right) + s^2\left(\cos^{-1}\frac{e^2 + s^2 - r_k^2}{2es}\right) - \frac{1}{2}\sqrt{(-e + r_k + s)(e + r_k - s)(e - r_k + s)(e + r_k + s)} \tag{19}$$

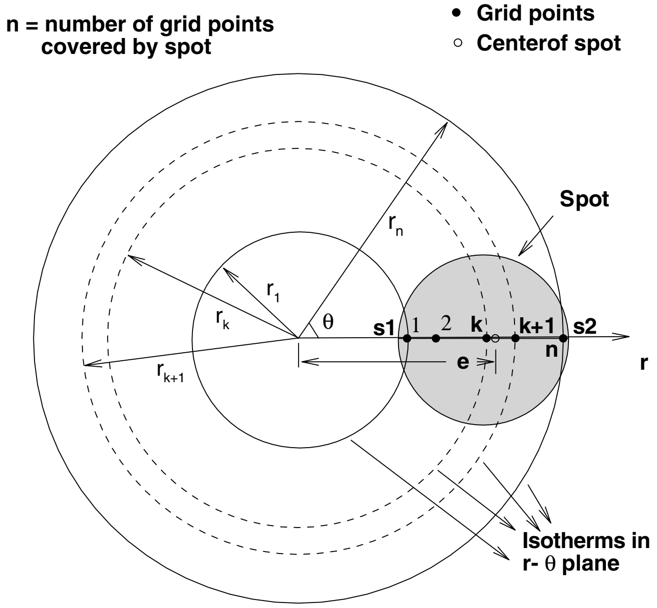

Fig. 8. Geometry used to calculate average temperature inside a laser measurement spot in r–θ plane.

Case II: If $r_k \leqslant |e - s|$, then

$$A_k = \pi r_k^2 \tag{20}$$

Fig. 9 compares the interface temperature obtained directly from the numerical simulation with the spatial-averaging procedure corresponding to a laser measurement (Eq. (18)) for all four liquids on the maximum extension of their spreading. The center location of the spatially averaged spots e is varied from 0 to $r_c - s$, with a resolution

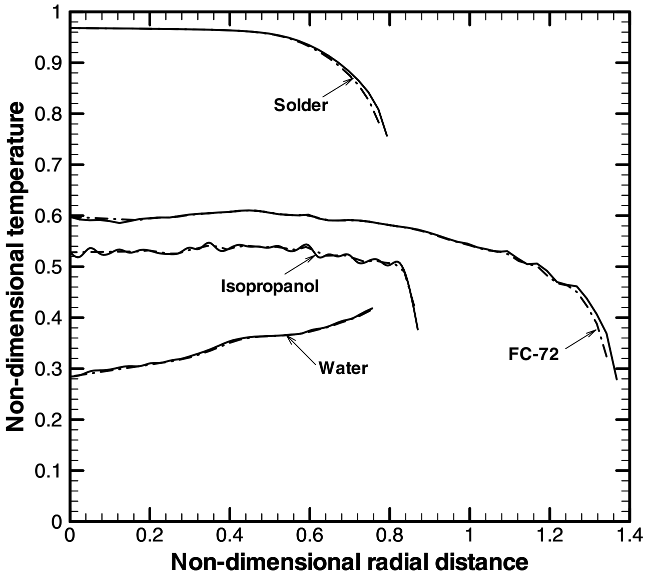

Fig. 9. Comparison of actual and spatially averaged temperature results simulating the measurement of a laser measurement spot size of 15 μm $Bi = 100$. Solid line patterns show actual results while dashed line pattern denotes spatially averaged results.

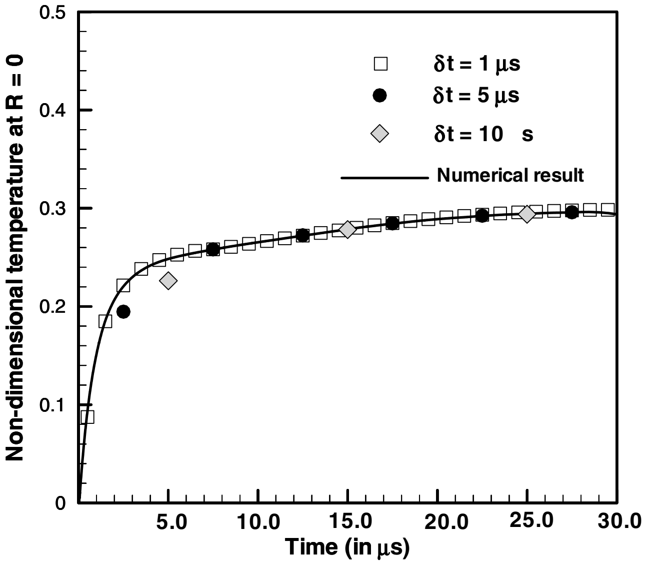

Fig. 10. Comparison of actual and time-averaged temperature results assuming a data acquisition time of 1, 5 and 10 μs, at the location $R = 0$ on interface (for water, $Bi = 100$). Solid line pattern shows actual result while symbols denote time-averaged results.

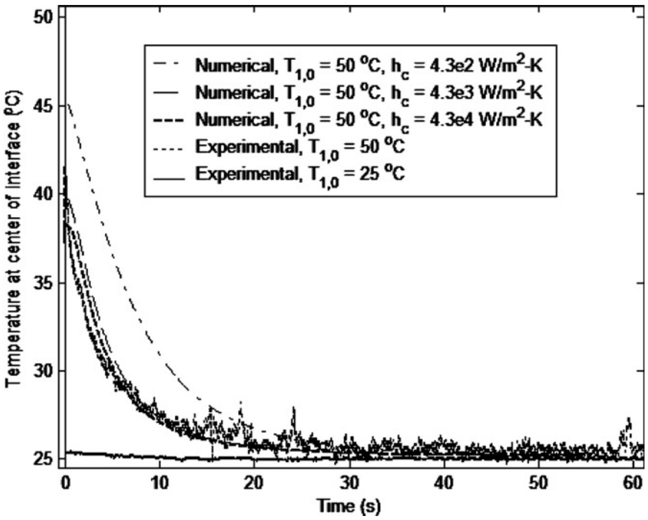

Fig. 11. Comparison between measurement and simulations of the average temperature of splat for complete cooling of 2.8 mm water drop. Initial temperature and impact velocity of the drop are 50 °C and 0.4 m/s, respectively.

of 1 μm. The actual and spatially averaged temperatures are shown as solid and dashed lines, respectively. In all cases the spatially averaged temperatures are in very good agreement with the numerical values. The numerical studies provide therefore insight into the uncertainty of the experiment.

Similarly, to estimate the uncertainty induced by a measurement with a temporal resolution of δt, corresponding to the available experimental setup, numerical temperatures are averaged within δt as follows:

$$T_{\text{avg,temporal}}\left(\frac{t_s + t_e}{2}\right) = \frac{1}{\delta t}\int_{t_s}^{t_e} T(t)\,\mathrm{d}t \tag{21}$$

where t_s and t_e are the start and end time within which the temperature value is measured and $t_e - t_s = \delta t$.

Fig. 10 shows the evolution of the interface temperature at $R = 0$ as a function of time for water. The solid curve shows the numerical results while the symbols simulate a temperature measurement with $\delta t = 1, 5$ and 10 μs. It appears that any of these resolutions is suitable for the temperature measurement at times larger than 7 μs after impact.

5.3. Comparison with experimental results

This modeling will be used to determine values of interfacial heat transfer coefficient, by matching numerical temperatures at the droplet–substrate interface with temperature measurements. This matching process is illustrated in Fig. 11, in a similar matching process used during the impact of mm-size drops on a glass surface. In Fig. 11, temperatures simulated and measured are obtained for a 2.8 mm diameter water drop and a fused silica substrate. Initial temperature and impact velocity of the drop are 50 °C and 0.4 m/s, respectively. When the warm droplet impacts a surface at a colder temperature, heat is transferred from the drop by convection and conduction. In Fig. 11, average temperatures of drop from several simulations are superposed to the experimental temperature (differential laser measurement), with values of interfacial heat transfer coefficient (h_c) ranging from 4.3×10^2 to 4.3×10^4 W/m^2-K. Our results show that the experimental and numerical cooling curves superimpose each other best for a value of interfacial heat transfer coefficient of 4.3×10^3 W/m^2-K (or higher).

6. Conclusions

A numerical investigation of the fluid mechanics and heat transfer for a liquid microdroplet impacting on a substrate at a different temperature has been performed. In particular the effects of interfacial heat transfer, droplet spreading, and temperature variation at the interface are assessed. The liquids investigated are eutectic lead–tin solder (63Sn–37Pb), water, isopropanol and FC-72. Among the liquids, the spreading of FC-72 is the largest because of its larger Weber number. The interfacial Biot number is shown to control the location of the onset of phase change: for instance phase change is shown to happen at the droplet periphery for solder and along the entire contact surface between droplet and substrate for water, isopropanol and FC-72, if the Biot number is sufficiently large ($Bi > 100$). The numerical results are compared with published experimental results as well as an elementary analytical analysis. A key objective of this work is to assess the feasibility of a novel laser-based measurement technique to measure interfacial temperature at the droplet–substrate interface, with a high temporal and spatial resolution of respectively 1 μs and 15 μm. To assess the feasibility of this technique, numerical results are used to predict the droplet spreading and temperature history. These numerical results are used to determine if the expected spatial and temporal limitations of the experimental technique will be sufficient to adequately resolve the transient temperatures at the droplet–substrate interface. The initial conclusions are that the experimental technique will be able to accurately capture the temperature history at the droplet–substrate interface, given the available temporal and spatial resolutions. The results also show that the eutectic solder is the best candidate to measure radial temperature variations, while FC-72 and isopropanol exhibit larger spreading diameters and thus are natural candidates for preliminary experiments.

Acknowledgements

The authors gratefully acknowledge financial support for this work from the Chemical Transport Systems Division of the US National Science Foundation through grant 0336757.

References

[1] H. Jones, Rapid Solidification of Metals and Alloys, vol. 8, Great Britain Institution of Metallurgists, London, 1982.

[2] S. Annavarapu, D. Apelian, A. Lawley, Spray casting of steel strip: process analysis, Metall. Trans. A 21 (1990) 3237–3256.

[3] D. Attinger, S. Haferl, Z. Zhao, D. Poulikakos, Transport phenomena in the impact of a molten droplet on a surface: macroscopic phenomenology and microscopic considerations. Part II: heat transfer and solidification, Ann. Rev. Heat Transfer XI (2000) 65–143.

[4] D.J. Hayes, D.B. Wallace, M.T. Boldman, Picoliter solder droplet dispension, in: ISHM Symposium 92 Proceedings, 1992, pp. 316–321.

[5] J.M. Waldvogel, G. Diversiev, D. Poulikakos, C.M. Megaridis, D. Attinger, B. Xiong, D.B. Wallace, Impact and solidification of molten-metal droplets on electronic substrates, J. Heat Transfer 120 (1998) 539.

[6] F.H. Harlow, J.P. Shannon, The splash of a liquid drop, J. Appl. Phys. 38 (1967) 3855–3866.

[7] K. Tsurutani, M. Yao, J. Senda, H. Fujimoto, Numerical analysis of the deformation process of a droplet impinging upon a wall, JSME Int. J. Ser. II 33 (1990) 555–561.

[8] M. Pasandideh-Fard, Y.M. Qiao, S. Chandra, J. Mostaghimi, A three-dimensional model of droplet impact and solidification, Int. J. Heat Mass Transfer 45 (2002) 2229–2242.

[9] F. Gao, A. Sonin, Precise deposition of molten microdrops: the physics of digital microfabrication, Proc. Roy. Soc. London A 444 (1994) 533–554.

[10] G.X. Wang, E.F. Matthys, Numerical modeling of phase change and heat transfer during rapid solidification processes, Int. J. Heat Mass Transfer 35 (1) (1992) 141–153.

[11] T. Bennett, D. Poulikakos, Heat transfer aspects of splat-quench solidification: modeling and experiment, J. Mater. Sci. 29 (1994) 2025–2039.

[12] Z. Zhao, D. Poulikakos, J. Fukai, Heat transfer and fluid dynamics during the collision of a liquid droplet on a substrate: I – modeling, Int. J. Heat Mass Transfer 39 (1996) 2771–2789.

[13] J. Fukai, Z. Zhao, D. Poulikakos, C.M. Megaridis, O. Miyatake, Modeling of the deformation of a liquid droplet impinging upon a flat surface, Phys. Fluids A 5 (1993) 2588–2599.

[14] J.M. Waldvogel, D. Poulikakos, D.B. Wallace, R. Marusak, Transport phenomena in picoliter size solder droplet dispension, J. Heat Transfer 118 (1) (1996) 148–156.

[15] J.M. Waldvogel, D. Poulikakos, Solidification phenomena in picoliter size solder droplet deposition on a composite substrate, Int. J. Heat and Mass Transfer 40 (2) (1997) 295–309.

[16] This routine was developed by Francis X. Giraldo at Naval Research Laboratory in Monterey, CA.

[17] W. Liu, G.X. Wang, E.F. Matthys, Determination of the thermal contact coefficient for a molten droplet impinging on a substrate, Transport Phenom. Mater. Process. Manuf. ASME HTD 196 (1992).

[18] M. Pasandideh-Fard, J. Mostaghimi, On the spreading and solidification of molten particles in a plasma spray process: effect of thermal contact resistance, Plasma Chem. Plasma Process. 16 (1996) 83–98.

[19] B. Xiong, C.M. Megaridis, D. Poulikakos, H. Hoang, An investigation of key factors affecting solder microdroplet deposition, J. Heat Transfer 120 (1) (1998) 259–270, 1998.

[20] D. Attinger, D. Poulikakos, On quantifying interfacial thermal and surface energy during molten microdroplet surface deposition, J. Atom. Spray 13 (218) (2003) 309–319, 2003.

[21] Q. Chen, Y. Li, J.P. Longtin, Real-time laser-based measurement of interface temperature during droplet impingement on a cold surface, Int. J. Heat Mass Transfer 46 (5) (2003) 879–888.

[22] P. Bach, O. Hassager, An algorithm for the use of the Lagrangian specification in Newtonian fluid mechanics and applications to free-surface flow, J. Fluid Mech. 152 (1985) 173–190.

[23] S. Haferl, Z. Zhao, J. Giannakouros, D. Attinger, D. Poulikakos, Transport phenomena in the impact of a molten droplet on a surface: macroscopic phenomenology and microscopic considerations. Part I: fluid dynamics, in: C.L. Tien (Ed.), Annual Review of Heat Transfer, Begell House, NY, 2000, pp. 145–205.

[24] G.X. Wang, E.F. Matthys, Modeling of heat transfer and solidification during splat cooling: effect of splat thickness and splat/substrate thermal contact, Int. J. Rapid Solidifi. 6 (1991) 141–174.

[25] J. Peraire, M. Vahdati, K. Morgan, O.C. Zienkiewicz, Adaptive remeshing for compressible flow computations, J. Comput. Physics 72 (1987) 449–466.

[26] M. Dietzel, S. Haferl, Y. Ventikos, D. Poulikakos, Marangoni and variable viscosity phenomena in picoliter size solder droplet deposition, J. Heat Transfer 125 (2003) 365.

[27] CRC Handbook of Chemistry and Physics.

[28] C.K. Chow, D. Attinger, Visualization and measurements of microdroplet impact dynamics on a curved substrate, in: ASME_JSME Joint Fluids Engineering Conference, Honolulu, Hawai, ASME, New York, 2003.

[29] Y.A. Cengel, Heat Transfer: A Practical Approach, second ed., Mc Graw Hill, NY, 2003.

[30] http://mathworld.wolfram.com/Circle-CircleIntersection.html.